IEEE Access
Multidisciplinary | Rapid Review | Open Access Journal

Received 7 February 2023, accepted 27 February 2023, date of publication 6 March 2023, date of current version 10 March 2023.

Digital Object Identifier 10.1109/ACCESS.2023.3253392

RESEARCH ARTICLE

Multi-Objective Design Optimization for HVDC-LCC Converter Transformers: Analytical and FEA-Based Comparison

MARCOS V. CZERNORUCKI[1,3], MAURICIO BARBOSA DE CAMARGO SALLES[1], (Member, IEEE), SÉRGIO LUCIANO AVILA[1,2], FELIPE ALVES SOBRINHO[3], WILERSON W. CALIL[3], AND JOSÉ ROBERTO CARDOSO[1], (Life Member, IEEE)

[1]Laboratory of Advanced Electric Grids (LGRID), Polytechnic School of the University of São Paulo, São Paulo 05508-010, Brazil
[2]Laboratory of Applied Scientific Computing (PECCE), Federal Institute of Santa Catarina, Florianópolis 88020-300, Brazil
[3]Hitachi Energy Ltd., Guarulhos 07190-904, Brazil

Corresponding author: Sérgio Luciano Avila (Sergio.Avila@ifsc.edu.br)

This work was supported by the Coordenação de Aperfeiçoamento de Pessoal de Nível Superior-Brazil (CAPES) - Finance Code 001.

ABSTRACT The emerging HVDC technology has been used for long-distance power transmission, increasing flexibility to the power systems, handling asynchronous interconnections, crossing long-distance submarine cables, unusual loading, and generation profiles, and improving energy market relations. The HVDC converter transformers are designed based on system parameters, that directly affect the core and windings geometries, thus the weight and operating losses. In a standard design process, the designer adjusts the active part dimensions, until the constructive and specified aspects, moreover, the technical standard restrictions, are satisfied. The main contribution is to formulate analytic equations, in a way that losses and weight can be obtained for several options of core and windings geometry. However, weight and losses are opposite objectives in the search for an optimal solution. Understanding this compromise between opposing goals is relevant to the equipment learning process. In this context, another significant contribution of the work is to carry out a formal optimization process through the analytical formulation developed. To minimize the weight and operating losses, and subject to IEC standards and constructive restrictions, the multi-objective Genetic Algorithm has been used to search for the Pareto Frontier. Far beyond the chosen solution, the non-dominated frontier obtained for each transformer design, allows the designer to learn about the equipment and its operation, leading to a continuous improvement of the proposed methodology. The analytical formulation is validated by an alternative numerical methodology for winding harmonic losses and short-circuit impedance verification, providing meaningful confidence for the applied method.

INDEX TERMS HVDC, transformer, design, losses, optimization.

I. INTRODUCTION

The HVDC systems are implemented worldwide as a reliable solution for bulk energy transportation through long overhead lines, and underground or submarine cables. It has been recognized as a competitive alternative for AC transmission, integrating different sources of energy, increasing the electrical system reliability and power quality. Renewable sources integrate an important share of the actual global energetic matrix, contributing to the global carbon generation drop [1], and HVDC technology has permitted systems and countries' interconnection for power exchange, likewise connecting offshore wind farms, oil and gas platforms for energy generation and consumption.

Thus, designing and manufacturing an HVDC system and its equipment demand special expertise and require great investment for implementation. The converter transformer is considered a fundamental part of this investment and the main drive for system efficiency. Hence, optimizing the transformer design, especially in terms of losses and weight, is a

The associate editor coordinating the review of this manuscript and approving it for publication was Ali Raza.

TABLE 1. HVDC System Data From the PSCAD Simulations.

MW	AC [kV]	DC [kV]	Current [A]	Line length [km]
4000	500	800	2500	2500

valuable engineering task. The design optimization process must consider several other requirements from the technical specification, that cannot be neglected. This work proposes an analytic formulation for converter transformers design defined for a classic ±800 kV LCC (line-commutated converter) link, for the rectifier and inverter stations. The transformers' valve windings are connected in delta and wye at each station. This winding is also directly affected by the current harmonics since it is physically connected to the converter valves.

The standard design solution to define an optimal active part (core and windings) geometry which fulfils the desired objectives would require carrying out multiple design options, comparing them individually. Applying optimization algorithms over the analytical formulation, several applicable solutions are presented at once for each design type and the most suitable solution is selected. A multi-objective exercise is performed using the HVDC transformers designs, obtaining a Pareto's set of solutions, presented graphically, assisting the designer to select the most suitable option among several choices.

The work provides a consistent analytic formulation for HVDC transformers, validated by the valve winding losses analysis by a numerical alternative methodology. Moreover, the short-circuit impedance magnitude is verified providing confidence to the method.

A. GENERIC HVDC LCC SYSTEM

The HVDC system influences the transformer design through several effects, intrinsic to the converters switching, or to the system operation, which are widely described in the references [2] and [3]. The AC-DC-AC current conversion results in current harmonics that circulate directly through the transformer windings. The selected system for the study was the Belo Monte link located in Brazil rated at U_d±800 kV DC voltage, bipole, 2500 km overhead line length, 4000 MW rated power and 2500 A rated current (I_d) [4]. The 500 kV at line side, single-phase, two-winding transformers were modeled and connected to the twelve-pulse converters [5]. A bank of three single-phase transformers is connected to each six-pulse bridges: one bank has the secondary connected in star and the other in delta. A generic HVDC link model and transformers parameters were adjusted according to the Belo Monte system characteristics. The harmonic current spectrum of this HVDC bipole model was obtained using PSCAD [6] and considering a 1.5% DC voltage drop along the line. The rectifier converter is modeled with a 15° firing angle while the inverter converter had an extinction angle of 17°. The detailed system parameters are given in Table 1.

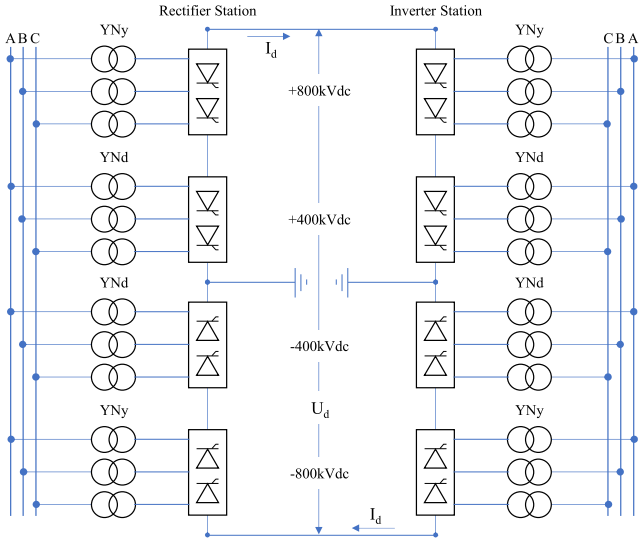

FIGURE 1. The simplified generic circuit used for the simulation in PSCAD [4].

TABLE 2. HVDC Transformers Parameters From the PSCAD Simulations.

Station	S_{base} [MVA]	AC wdg [kV]	DC wdg [kV]	Connection	Rated Impedance [%]
Inverter	376.7	500/√3	319.6	YN/d	15.0
	376.7	500/√3	319.6/√3	YN/y	15.0
Rectifier	393.5	500/√3	333.9	YN/d	15.0
	393.5	500/√3	333.9/√3	YN/y	15.0

The firing angle defines the harmonic content in the load current. The angle magnitude may assume distinct values according to the DC voltage level, overload profile, and line voltage drop. The simplified generic circuit is shown in Fig. 1 and the detailed transformer parameters are given in Table 2.

The converter transformers are identified according to the rectifier (on the left side) and the inverter stations (on the right side), based on the valve winding connection. The delta transformer (YNd) is connected after the lower DC voltage stage at ± 400 kVdc and the wye transformer (YNy) after the ± 800 kVdc level. The 500 kVac line windings are wye connected with an on-load tap changer (OLTC) with 31 electrical positions [7], for all transformers. The AC system frequency is 60Hz and the impedances are 15% at rated voltage and power. The transformers of the rectifier station are single-phase, with a rated power of 393.5 MVA and 333.9 kV voltage on the valve side. On the inverter side, the transformers are single-phase, 376.7 MVA and 319.6 kV valve winding voltage.

B. CONTENT OF THE SECTIONS

Along the coming sections the authors bring design considerations for the transformer active part dimensions definition (section II) and propose an analytical formulation to calculate the active part weight and converter transformer losses (section III). Further, the formulation is used to seek

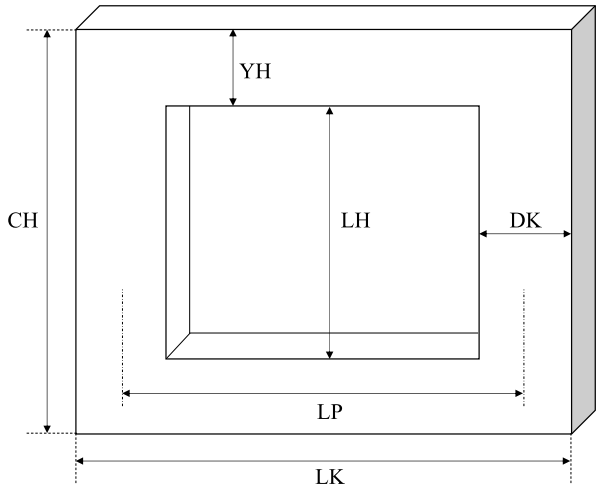

FIGURE 2. Single-phase core design main parameters.

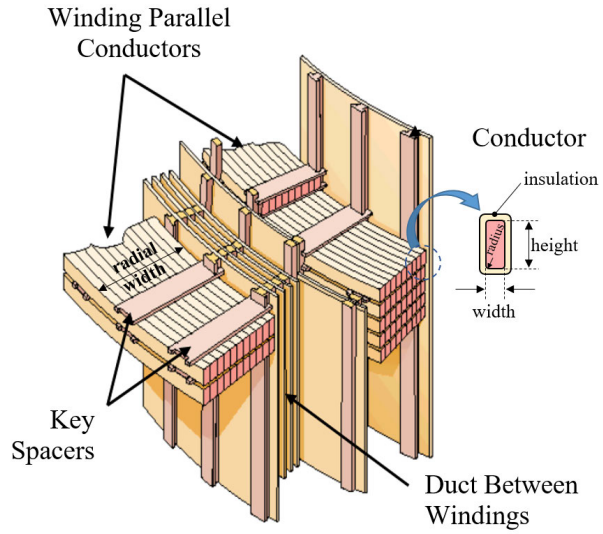

FIGURE 3. Winding and conductors' design, adapted from [9].

an optimal solution (section IV) in terms of weight and losses using multi-objective optimization. Finally, the analytic formulation is validated by a numerical model using the Finite Element Method to calculate the winding losses and the short-circuit impedance verification (section V).

II. TRANSFORMER DESIGN CONSIDERATIONS

The transformer active part design consists basically of the core and windings' geometrical dimensions definition. Both are influenced by specified requirements such as power, voltages, impedance, dielectric tests, overvoltage, overloads, etc. [3] The core dimension definition will restrict the region inside the core window, called limb height. The winding block is placed inside the core window, and the windings' geometry defines the core limb pitch. Thus, the core and winding designs are closely linked, and the parameters' variation affects the complete active part design. That interdependence can be visualized in Figs. 2, 3 and 6.

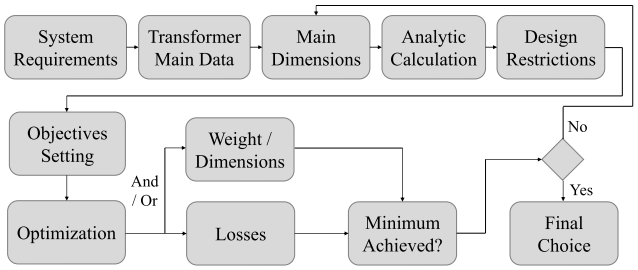

FIGURE 4. Flowchart of a conventional transformer design.

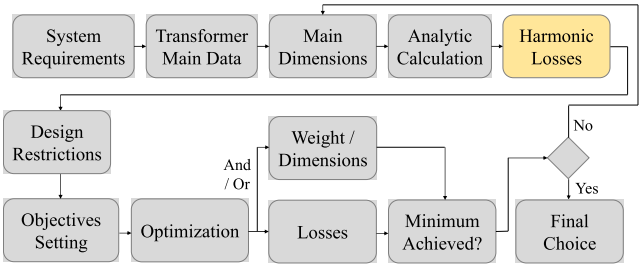

FIGURE 5. Flowchart of a converter transformer design.

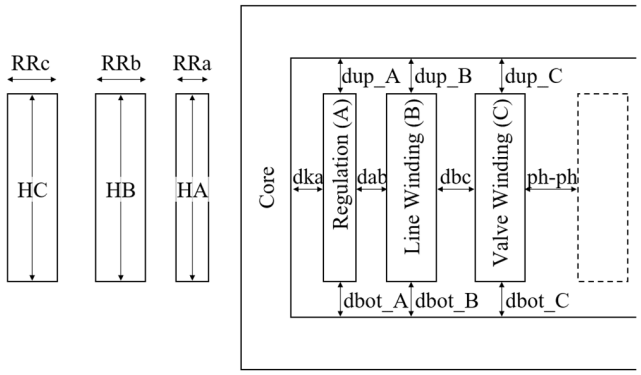

FIGURE 6. Cross-section view of one core limb representing the windings' layout and distances.

A. MAIN DIMENSIONS DEFINITION

The core design defines the geometry of the magnetic circuit, which is given by the diameter (DK), limb height (LH), limb pitch (LP), core height (CH), yoke height (YH), and core length (LK). The limb height is defined by the windings height and the distances to the yokes, top, and bottom, which are a result of the dielectric tests, service voltages, and mechanical or magnetic requirements. A simplified geometry of a single-phase core, with two wound limbs, like the one used in the actual study, is given in Fig. 2.

The winding design is defined by the winding inner diameter (D_w), axial height (H_w), and radial width (RR). The windings are concentric and assembled around the two core limbs. The winding conductor is defined by its height (h_c), width (rr), radius (rd), and paper insulation ($insul$). The turns can be separated by key spacers and the windings by radial ducts filled with insulating material. The number of turns ($turn$) defines the winding height (H_w), and the number of parallel conductors ($paral$) defines the radial width (RR). Details are shown in Fig. 3.

A simplified formulation is presented in section II-D, based on [8], to define the geometry of the core, windings, and conductors. For a specific geometry the core and copper weight, and the total losses in operation, including current harmonics are calculated.

The coming sections provide the reader an overview of the difference between a conventional and a converter transformer design.

B. CONVENTIONAL TRANSFORMER DESIGN

The conventional transformer design begins with a technical specification analysis, where the system voltages are defined for the high and low voltage sides, frequency, and other requirements relevant to the transformer design. In the same specification, the transformer's main data are provided, such as the number of phases, rated power, tap changer location, tap range, short-circuit impedance, losses, dimensions, and weight limitations. Based on that information combined with the applicable technical standards (IEC, IEEE, etc.), the engineer will start the transformer design fixing some parameters and leaving others free, to define the core and windings main dimensions, given in Fig. 2.

Designing a transformer can be an optimization exercise, based on restrictions given by the specification and technical standards, to achieve the most suitable option that fulfills the given objectives, which can be minimum weight, dimensions, or losses. It can also be a combination of two or more given objectives [8]. Figure 4 shows a conventional transformer design basic flowchart.

C. CONVERTER TRANSFORMER SPECIAL REQUIREMENTS

The converter transformer design must take into account several undesired effects related to the converters' non-linear operation, HVDC system voltage variation and loading, DC bias effect [10], noise level, and electric field distribution [2] and [3]. For losses calculation, the main effect to be considered in the design is the load losses increase due to the harmonic spectrum generated by the converters' operation. Such calculation methodology is clearly explained in section III-C.

According to the technical specification of the Belo Monte link [4], the transformers shall be designed for a 133% long-term overload for 30 minutes and 150% short-term emergency for 5 seconds. Those conditions, in a two-bipole installation, represent the loss of one monopole or one bipole respectively, and the time is defined by the control system to rearrange the load, avoiding a forced disconnection. During the optimization in section IV, that loading profile was represented as a daily cycle, to be applied as an overcurrent input into the models.

D. MAIN DIMENSIONS CALCULATION

The study presented in this work was performed varying two core parameters within a certain range: the limb height (LH), and the core diameter (DK). Some parameters were kept fixed since their determination is not related directly to the study purpose. The radial ducts (dka, dab and dbc), axial ducts toward the yokes (dup_A, dup_B, dup_C, $dbot\_A$, $dbot\_Banddbot\_C$), distance between winding blocks ($ph-ph$), conductor insulation ($insul$) and key spacers thickness ($spactk$), which are directly related to the system insulation coordination [11]. Those distances are represented in a cross-section of the core window in Fig. 6, together with the windings' layout, being illustrated, from the core limb, the regulation (A), line (B), and valve (C) windings. The single-phase core has two wounded limbs, and the winding blocks are connected in parallel. Figure 6 represents the winding block of only one wounded limb. The conductor corner radius (rr) and the number of parallel conductors ($paral$) are used for the conductor's dimensions definition. The core flux density (ϕ) is defined by the overvoltage requirements, saturation, and core steel material. It certainly affects the core losses, but for the study, the total losses, no-load, and load losses including harmonics and overload profile are analyzed and restricted together.

TABLE 3. Symbols used in the Formulation.

	CORE		WINDING
DK	core diameter	RR	radial width
CH	core height	H_w	axial height
YH	yoke height	$spactk$	spacer thickness
LH	limb height	A_w	cross-section area
LP	limb pitch	$paral$	cables in parallel
LK	core length	$turn$	number of turns
		$ndisc$	number of discs
	ACTIVE PART	$turnd$	turns per disc
dka	dist. core wdg A	D_w	inner diameter
dab	dist. wdg A to B		
dbc	dist. wdg B to C		CONDUCTOR
ph_ph	dist. between phases	rr	radial width
dup	upper dist. yoke wdg	h_c	axial height
$dbot$	bottom dist. yoke wdg	rd	corner radius
		$insul$	insulation thickness

The windings' cross-section areas (A_w) are related to the windings' current density, which was kept the same. Depending on the connection of the delta and wye valve windings, the phase voltage will assume different values by $\sqrt{3}$ relation, which defines the number of turns and the winding type. Helical and layer windings are the ones where each round represents one turn, therefore, the turn per disc ($turnd$) is equal to one. The number of parallel cables ($paral$) defines the winding radial width (RR). A disc winding type can have several turns in the same disc, and the radial width is defined by the number of parallel cables ($paral$) combined with the number of turns per disc ($ndisc$) [12]. The symbols used for each parameter described are detailed in Table 3.

Since the core flux density is defined, the windings' number of turns can be determined for each DK input, by (1).

$$N = \frac{V}{4.44 f N \emptyset A_k} \tag{1}$$

where,

V: phase voltage [V]
f: frequency in [Hz]
N: number of turns
ϕ : flux density in [T]
A_k: core cross-section area in [m^2]

The cross-section area A_k (2) is calculated by the core diameter and the core space factor k_s, which was defined as 0.898, considering some fiberglass insulation, core bandage, and structure material such as flitch plates [8].

$$A_k = \frac{\pi \left(DK10^{-3}\right)^2}{4} k_s \tag{2}$$

The total winding height in [mm] is given by (3) and the number of discs, by (4).

$$H_w = LH - dup - dbot \tag{3}$$
$$ndisc = N/turnd \tag{4}$$

The conductor copper height and width in [mm] are calculated by (5) and (6). For layer windings, like the regulating (A), spactk is null. The conductors' radius is according to the supplier rules. For this study, the conductors for winding A and B used a 1.0mm radius and winding C, 0.5mm.

$$hc = \frac{[H_w - spactk\ (ndisc - 1)] - insul\ ndisc}{ndisc} \tag{5}$$
$$rr = \frac{(A_w/paral) + rd^2\ (4 - \pi)}{hc} \tag{6}$$

Finally, the winding radial width in [mm] is calculated by (7).

$$RR = (rr + insul)\, paral\ turnd \tag{7}$$

The windings' inner diameters D_w in [mm] are given by (8).

$$\begin{aligned} D_{wA} &= DK + dka \\ D_{wB} &= D_{wA} + 2RR_A + dab \\ D_{wC} &= D_{wB} + 2RR_B + dbc \end{aligned} \tag{8}$$

The core length in [mm] is defined by (9). The yoke height is equal to the core diameter and the limb pitch is given by (8).

$$LK = DK + 2\,(D_{wC} + 2RR_C) + ph\_ph \tag{9}$$
$$LP = 2\,(D_{wC} + RR_C) + ph\_ph \tag{10}$$

This basic formulation defines the geometry of the core, windings, and conductors for the several DK and LH as input.

III. ANALYTICAL FORMULATION FOR CONVERTER TRANSFORMER

From the geometry defined by the core and windings' main dimensions' calculation, the magnetic no-load losses, the load losses, and the short circuit impedance can be calculated in the coming sections. As mentioned before, the converter transformer in operation is affected by the current harmonics generated by the power electronics elements switching, increasing specifically the additional load losses [13]. That design consideration is explained further in sections III-C and D.

TABLE 4. Core steel material magnetic losses [8].

Flux density [T]	Magnetic losses [W/kg]
0,20	0,022
0,30	0,048
0,40	0,082
0,50	0,124
0,60	0,174
0,70	0,231
0,80	0,297
0,90	0,370
1,00	0,452
1,10	0,542
1,20	0,643
1,40	0,886
1,60	1,210
1,70	1,463
1,80	1,867
1,85	2,122

A. CORE WEIGHT AND LOSSES

The magnetic losses related to the core steel material are given by the supplier in terms of W/kg, depending on the flux density in [T], according to Table 4. The losses due to the Foucault effect were neglected. The core weight G_{Fe} in [kg], is calculated by the mean magnetic path length in (11), based on the variables defined before, the number of core limbs (n_{limb}), and the steel volumetric density d_{fe} (7650 kg/m^3) [14].

$$G_{Fe} = [2LK + n_{limb}\,(LH + YH)]\, A_k d_{fe} 10^{-3} \tag{11}$$

Thus, the core losses are a result of the product of the weight G_{Fe} times the magnetic losses P_{mag} (12).

$$P_0 = G_{Fe} P_{mag} \tag{12}$$

For the actual study a core flux density of 1.70 T was chosen, once the specification had a limitation in sound level, which would not allow the designer to go close to the material saturation limit.

Although, higher or lower flux density values may be chosen depending on other specification requirements like no-load losses, flux density limitations, overvoltage, underfrequency, or reactive loadings.

B. WINDING LOSSES AND TOTAL WEIGHT

The transformer winding losses are divided into two specific components: i) resistive losses, which are the most significant loss component in power transformers, originated from the windings' resistance, and also known as ohmic losses; ii) additional losses, resulted by eddy currents circulation in

the conductors exposed to the magnetic field [15]. Both loss components define the winding load losses.

The converter transformer load current is composed of the fundamental frequency component and different harmonic orders [14], which can assume distinct profiles depending on the HVDC installation and the system operation modes. That harmonic influence affects the additional losses [16]. The load losses are also intrinsically related to the transformer impedance, which represents the part of the energy contained in the leakage magnetic flux. Converter transformers for LCC applications normally are specified with considerably high impedances, to contribute with the HVDC short-circuit power strength, limiting the fault currents. Hence, the contribution of the magnetic flux to the total converter transformer load losses is extremely significant [17].

From the geometry defined in section II-D, the winding cross-section area is used to calculate the winding resistance R_w in [Ω] (13), based on the winding inner diameter, radial dimension, number of turns, and copper resistivity (2.09 10^{-8} [Ω-m]).

$$R_w = (D_w + RR)10^3 \pi N \rho \Big/ A_w \tag{13}$$

And the ohmic losses in [W] are calculated based on the winding load current I_w in (14) for a certain reference temperature, T_{ref}.

$$P_{RI^2} = R_w I_w^2 \frac{(234.5 + T_{ref})}{234.5 + 75} \tag{14}$$

The reference [18] contains analytic equations used in this work to calculate the theoretical winding load losses. The peak leakage flux B_0 in [T] is generated by the windings and its magnitude is defined as a function of the transformer ampere-turn (NI), the winding height, and the winding radial dimension, presented in (15).

$$B_0 = \mu_0 H = \frac{\mu_o \sqrt{2} NIRR}{H_w} \tag{15}$$

Being $\mu_0 = 4\pi\ 10^{-7}$ in the SI system. The winding loss volumetric density P_e in [W/m^3] can be calculated by (16), it is obtained from the frequency, the winding leakage flux, and the conductor radial width for axial losses calculation or axial height for radial losses [19].

$$P_e = \left(\frac{\pi^2}{6}\right) \frac{f^2 B_0^2 b^2}{\rho} \tag{16}$$

where b is equal to rr for axial losses, and to h_c for radial losses. The conductor cross-section area in [m^2] is given by (17):

$$a_c = h_c rr - rd^2 (4 - \pi)\, 10^{-6} \tag{17}$$

The magnetic flux impinging the conductor cross-section area creates a Foucault current loop. The presence of a flowing current affects the flux behavior about various points in the section, but the magnetomotive force is found to be canceled when calculated around a spot. That fact would demand an enormous amount of labor to achieve a correction factor which would represent that effect in additional losses and impedance calculation. That was performed by dr. Rogowski [20] in the past, who defined a factor that can be applied for such a purpose.

In a simplified approach, the Rogowski factor K_r for a transformer that has $H_r/\pi \dot{H}_w < 0.25$, where H_r is the geometric region of the leakage flux, defined on the ampere-turn diagram according to Fig. 5, and $\dot{H}_w$ is considered the average windings' height, can be defined in (18) as:

$$K_r = 1 - \frac{H_r}{\pi \dot{H}_w} \tag{18}$$

Finally, the winding additional eddy losses, P_{eddy}, in [W] can be obtained as defined in (19):

$$P_{eddy} = \pi\ (D_w + RR)\ 10^{-6}\ paral\ N a_c P_e K_r \tag{19}$$

The eddy losses together with the winding ohmic losses (RI^2) result in the total winding load losses, for a defined loading condition [19].

By the windings' geometry defined in section II-D, it is possible to calculate the windings' weight in [kg] using (20), the copper volumetric density is $\sigma = 8.93$ [g/cm^3].

$$G_{Cu} = N A_w\ (D_w + RR)\ \pi \sigma\ 10^{-6} \tag{20}$$

Thus, the core and copper weight to be analyzed will be the sum of (11) and (20), resulting in (21).

$$G_{tot} = G_{Fe} + G_{Cu} \tag{21}$$

C. IEC/IEEE 60076-57-129 TECHNICAL STANDARD

The HVDC transformers technical standard, IEC/IEEE 60076-57-129 [21], provides a formulation for total load losses calculation which has been used over the years to design and test converter transformers with success and extreme reliability, assured by the number of years HVDC projects have been running worldwide. It defines a multiplying factor F_{WE}, presented in (22), to represent the eddy losses increase due to the harmonics, also found in [22] and [23], defined as:

$$F_{WE} = \sum_{h=1}^{n} k_h^2 h^2$$
$$\text{Being } k_h = \frac{I_h}{I_r} \text{ and } h = \frac{f_h}{f_1}. \tag{22}$$

The technical standard [21] recommends that all current harmonic orders, h, up to the 49$^{\text{th}}$ shall be considered for the factor's determination. Different harmonic spectra may be informed to the manufacturer for several loading or overloading conditions. The currents I_h and I_r are respectively the magnitudes of the h^{th} harmonic and the rated in-service current for a specific load condition. The frequencies f_h and f_1 are the harmonic order and rated, which is also the fundamental frequency. The calculated winding losses for a conventional power transformer are obtained by (23) and for

TABLE 5. Harmonic Spectrum for the Inverter Station.

	Inverter Delta			Inverter Wye		
h	I_h [A]	k_h [pu]	$k_h^2h^2$	I_h [A]	k_h [pu]	$k_h^2h^2$
1	1929.73	0.945	0.893	1929.85	0.945	0.894
5	349.13	0.171	0.731	349.15	0.171	0.731
7	226.76	0.111	0.605	226.79	0.111	0.605
11	95.44	0.047	0.264	95.44	0.047	0.264
13	65.40	0.032	0.173	65.39	0.032	0.173
17	17.11	0.008	0.020	17.10	0.008	0.020
19	11.58	0.006	0.012	11.59	0.006	0.012
23	17.91	0.009	0.041	17.92	0.009	0.041
25	15.30	0.007	0.035	15.34	0.008	0.035
29	13.53	0.007	0.037	13.53	0.007	0.037
31	11.20	0.005	0.029	11.22	0.005	0.029
35	3.66	0.002	0.004	3.67	0.002	0.004
37	3.34	0.002	0.004	3.30	0.002	0.004
41	4.24	0.002	0.007	4.24	0.002	0.007
43	5.56	0.003	0.014	5.55	0.003	0.014
47	5.15	0.003	0.014	5.15	0.003	0.014
49	4.86	0.002	0.014	4.69	0.002	0.013
	F_{WE}		2.897			2.897

TABLE 6. Harmonic spectrum for the rectifier station.

	Rectifier Delta			Rectifier Wye		
h	I_h [A]	k_h [pu]	$k_h^2h^2$	I_h [A]	k_h [pu]	$k_h^2h^2$
1	1934.01	0.947	0.898	1933.93	0.947	0.898
5	347.86	0.170	0.726	347.73	0.170	0.725
7	222.04	0.109	0.580	222.11	0.109	0.580
11	89.94	0.044	0.235	89.94	0.044	0.235
13	62.96	0.031	0.161	62.94	0.031	0.161
17	18.78	0.009	0.024	18.80	0.009	0.025
19	11.41	0.006	0.011	11.46	0.006	0.011
23	19.31	0.009	0.047	19.32	0.009	0.047
25	16.27	0.008	0.040	16.24	0.008	0.040
29	13.26	0.006	0.035	13.24	0.006	0.035
31	8.93	0.004	0.018	8.89	0.004	0.018
35	3.44	0.002	0.003	3.46	0.002	0.004
37	2.91	0.001	0.003	2.92	0.001	0.003
41	5.81	0.003	0.014	5.81	0.003	0.014
43	5.49	0.003	0.013	5.49	0.003	0.013
47	4.35	0.002	0.010	4.35	0.002	0.010
49	3.81	0.002	0.008	3.94	0.002	0.009
	F_{WE}		2.828			2.828

a converter transformer are given by (24).

$$P_w = R_w I_w^2 + P_{eddy} \tag{23}$$

$$P_w^h = R_w I_w^2 + P_{eddy} F_{WE} \tag{24}$$

D. TOTAL LOSSES

The total losses including harmonics in [W] are given by (25), representing the sum of (12) and (24):

$$P_{tot}^h = P_0 + R_w I_w^2 + P_{eddy} F_{WE} \tag{25}$$

The HVDC system described in section I was simulated using the software PSCAD and the harmonic spectrum was determined for the rectifier and the inverter wye and delta transformers. The harmonic currents I_h obtained are presented in Tables 5 and 6, and the factor F_{WE} obtained per (22).

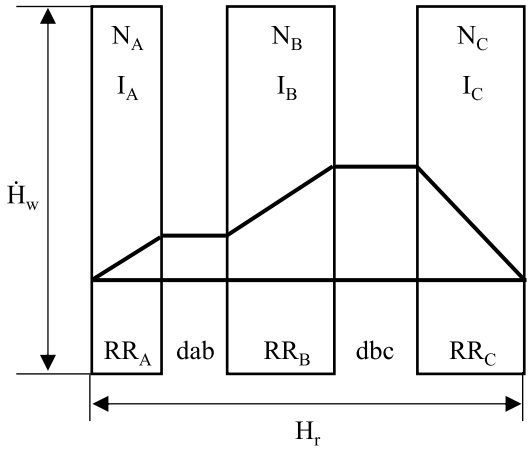

FIGURE 7. Ampere-turn diagram considered for Rogowski factor calculation.

E. IMPEDANCE CALCULATION

The transformer impedance is a parameter to be continuously monitored during the design and especially for converter transformers, it must be well controlled within a strict tolerance. The impedance magnitude is related to the magnetic leakage flux created by the winding block. Hence, its contribution to the total converter transformer load losses, especially for eddy losses, is extremely significant [24]. As per Table 2, the transformers' impedance for this study was fixed at 15% at the MVA base. The geometric area is calculated for each winding and for the radial duct between windings. In these specific designs, all transformers are composed of three coils as shown in Fig. 6, and based on the ampere-turn diagram of Fig. 7, being (A) the regulating winding, (B) the line winding, and (C) the valve winding. The geometric areas in [m^2] sd_A, sd_0, sd_B, sd_1 and sd_C are calculated in (26):

$$\begin{aligned} sd_A &= (D_{wA} + RR_A)\,\pi\,\left(RR_A/3\right)10^{-6} \\ sd_0 &= (D_{wA} + 2RR_A + dab)\,\pi\,dab10^{-6} \\ sd_B &= (D_{wB} + RR_B)\,\pi\,\left(RR_B/3\right)10^{-6} \\ sd_1 &= (D_{wB} + 2RR_B + dbc)\,\pi\,dbc10^{-6} \\ sd_C &= (D_{wC} + RR_C)\,\pi\,\left(RR_C/3\right)10^{-6} \\ sd &= sd_A + sd_0 + sd_B + sd_1 + sd_C \end{aligned} \tag{26}$$

With the weighted area sd calculated, the leakage flux B_0 from (15), and the Rogowski factor [20], K_r, from (18), the percentage impedance [18], U_k, can be calculated by (27).

$$U_k = 100\frac{4.44\sqrt{2}B_0 sdNfK_r}{V} \tag{27}$$

Thus, by the equations presented in sections II and III, the core and windings geometry, losses, weight, and transformer impedance can be calculated by an analytic methodology. That formulation was written into a commercial simulation software to perform the optimization exercises presented in section IV.

IV. DESIGN OPTIMIZATION

The parameters from Table 2 were used as input for the analytic formulation of the four converter transformers' designs. The winding type, number of turns, winding height and width, conductor cross-section area, and number of parallel cables vary according to the three-phase bank connection in wye or delta and depend on the power and voltage level of the rectifier or inverter station. The core height (CH), consequently, the limb height (LH), and the core diameter (DK), were limited by the practical transformer factory experience. That includes the commercial lifting crane and the vapor-phase oven height, combined with a maximum transport height limitation. The windings' radial dimensions (RR) follow the common manufacturer's rules to accommodate the electrostatic ring and the pressboard yoke collars for the windings' end protection against the core yokes and between windings, as presented in [25] and [26]. Furthermore, the windings' cross-section areas were defined to result in a current density of around 3.0 A/mm^2 of the maximum current along the whole tapping range, which is considered a satisfactory magnitude to comply with the overloading cycle, defined in [4].

A. THE PARETO-OPTIMAL SET DEFINITION

Optimizing an exercise means searching for the best solution to a given problem, limited by its physical-mathematical model [27], [28]. The model for a multi-objective optimization approach for the HVDC transformers designs can be written as (28):

$$\begin{aligned} &\text{To minimize } \vec{y} = \vec{f}(\vec{x}) = (y_1(\vec{x}), y_2(\vec{x})), \\ &\text{subject to } \vec{\boldsymbol{g}}\,(\vec{\boldsymbol{x}}) \text{ and} \\ &\qquad \vec{e}(\vec{y}) = (e_1(\vec{y}), e_2(\vec{y})) \leq 0 \end{aligned} \tag{28}$$

With,

$$\vec{y} = (G_{tot}, P^h_{tot}) \in Y^2 \text{ and } \vec{x} = (LH, DK) \in X^2$$

Being $\vec{\boldsymbol{y}}$ the objectives vector, Y the objectives space (two dimensions), $\vec{\boldsymbol{x}}$ the parameters vector, and X the parameters space (two dimensions). The parameters' restrictions $\vec{\boldsymbol{g}}(\vec{\boldsymbol{x}})$ are the limits, given in (32). The restrictions of the objectives $\vec{\boldsymbol{e}}(\vec{\boldsymbol{y}})$ were defined by the transformer short circuit impedance tolerance and the total losses including harmonics limitation, given in (29):

$$\begin{aligned} e_1\,(\vec{y}) &\rightarrow U_k = 15\% \pm 7.5\% \\ e_2\,(\vec{y}) &\rightarrow P^h_{tot} < S_{base} * 0.30\% \end{aligned} \tag{29}$$

The impedance restriction comes from the technical standard IEC 60076-1 [29] and the total losses were established based on [30], which is a local Brazilian norm applicable for large power transformers. The Pareto optimality concept is used for multi-objective modeling, understanding that two stated objectives, like G_{tot} and P^h_{tot}, are conflicting with each other. To reduce core and windings material with the same core type, winding layout, and material quality, the total losses will increase. It means that the improvement of one, implies the worsening of the other [27], [28]. Therefore, the optimization intends to find a solution that meets both objectives while respecting the given limits and restrictions. For a standard design process that could be achieved by several individual runs, comparing the results, until the optimal solution is reached. Using optimization algorithms, the solution can be presented together with other analyses in one single graphical representation. A possible solution $\vec{a} \in X_f$ (30) is called non-dominated if:

$$\nexists\, \vec{x} \in X_f : \vec{x} \succ \vec{a} \tag{30}$$

That is the main difference between the single-objective approach to multi-objective problems. There is not a single optimal solution but an optimal setting in which none can be identified as better without a new classification (e.g., preference for one of the objectives). The group of all non-dominated solutions is called a Pareto-optimal set [31]. By correspondence, the set of objective vectors forms the Pareto-optimal frontier [27]. In this context, optimization methods deal with a population of possible solutions that have the advantage of obtaining the Pareto-optimal set.

B. GENETIC ALGORITHM APPLICATION

The Genetic Algorithm (GA) is a stochastic optimization technique based on natural selection and genetics concepts [28], [31]. Solutions which generate new solutions are selected probabilistically according to their merits (obtained through an objective function that evaluates the quality of the individual for the problem (28)). The better the individual is, the greater his chances of reproducing (the greater is the probability of being selected and suffering genetic operators).

Some advantages of the GA can be highlighted, such as: the generation of a semi-optimal solutions list rather than a single solution, which is of great value for multi-objective optimization [32]. The evolutionary process and its multiple solutions help to understand the compromise between the conflicting objectives. For the proposed problem, the population of possible solutions can be written as (31):

$$Pop^n = \begin{bmatrix} LH^{n,1} & DK^{n,1} \\ \vdots & \vdots \\ LH^{n,nbind} & DK^{n,nbind} \end{bmatrix} \tag{31}$$

where each row represents an individual of the n^{th} generation, $nbind$ is the population size, and LH and DK are the two optimization parameters. The limb height varied from 1000 to 7000 mm, in steps of 10 mm, and the core diameter varied from 500 to 2000 mm, in steps of 1 mm. The core diameter range varies in smaller steps once, in practice, it is constructed by stacking the core steel sheets, which have tenths of millimeters thickness. The limb height is constructed in the longitudinal dimension of the magnetic steel sheet, which has many meters in length.

C. OPTIMIZATION RESULTS

The four exercises are large power transformers, that justify the limits selected in (32), which have upper

TABLE 7. Inverter Delta exercise.

Possible solutions	Non-dominated solutions (red bullet)		Dominated solutions (black points)	
	298		32877	
	Objectives		Parameters	
	G_{tot} x10^3[kg]	P^h_{tot} x10^3 [W]	LH [mm]	DK [mm]
Green	134.40	1346.2	5260	1018
Blue	194.30	1101.8	2460	1434
Cyan	182.50	1136.7	2550	1385
Final choice (white square)	147.30	1213.2	3990	1152

TABLE 8. Inverter Star exercise.

Possible solutions	Non-dominated solutions (red bullet)		Dominated solutions (black points)	
	235		34473	
	Objectives		Parameters	
	G_{tot} x10^3[kg]	P^h_{tot} x10^3 [W]	LH [mm]	DK [mm]
Green	162.71	994.81	6960	1002
Blue	215.39	831.66	3100	1423
Cyan	203.02	844.72	3210	1373
Final choice (white square)	181.36	867.26	4250	1228

TABLE 9. Rectifier Delta exercise.

Possible solutions	Non-dominated solutions (red bullet)		Dominated solutions (black points)	
	247		33033	
	Objectives		Parameters	
	G_{tot} x10^3[kg]	P^h_{tot} x10^3 [W]	LH [mm]	DK [mm]
Green	144.90	1136.0	6320	973
Blue	185.40	945.18	3050	1340
Cyan	178.20	975.37	3080	1309
Final choice (white square)	154.90	1019.60	4550	1120

and lower margins from the industry's common practice. The evolutionary-constrained multi-objective optimization methodology [31] has been performed several times. It is necessary due to its probabilistic nature. The process stop point happens when it is noticed the stagnation of the Pareto frontier.

$$\begin{bmatrix} LH \\ DK \end{bmatrix} = \begin{bmatrix} 1000 & 7000 \\ 500 & 2000 \end{bmatrix} \tag{32}$$

Figures 8 to 11 present all feasible solutions, according to (28), found until the stop point is reached for each exercise. Tables 7 to 10 present the solutions found for the lowest G_{tot} (green) and lowest P_{tot} (blue). Variation in objectives implies considerable variation in parameters. The solutions in magenta are those that respect a variation not greater than 0.25% around $U_k = 15\%$. For HVDC converter transformers it is a valuable strict restriction, once a deviation in the impedance within an HVDC link may result in unbalances and generation of even harmonics that were not considered in the original current spectrum. Among them, the one with the

TABLE 10. Rectifier Star exercise.

Possible solutions	Non-dominated solutions (red bullet)		Dominated solutions (black points)	
	251		34835	
	Objectives		Parameters	
	G_{tot} x10^3[kg]	P^h_{tot} x10^3 [W]	LH [mm]	DK [mm]
Green	167.80	1016.8	6790	1025
Blue	218.61	859.76	3210	1422
Cyan	211.08	874.43	3190	1397
Final choice (white square)	184.27	902.61	4470	1220

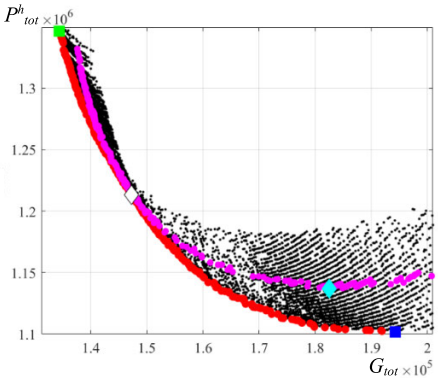

FIGURE 8. The feasible solutions found by the evolutionary constrained multi-objective optimization process for the inverter delta.

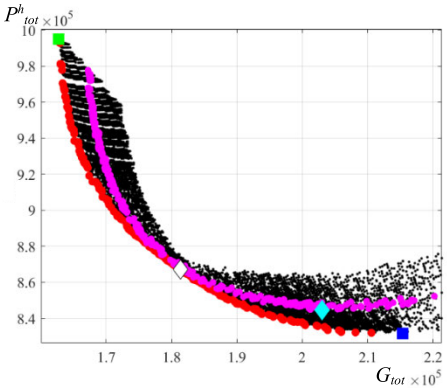

FIGURE 9. The feasible solutions found by the evolutionary constrained multi-objective optimization process for the inverter star.

lowest G_{tot} is highlighted as diamond cyan. These analyzes lead to a better understanding of the problem. A piece of better knowledge can point to the need of improving the model and/or to a more enlightened choice of the final solution [33].

Still respecting the tolerance reduction around U_k, the diamond white solution is the one closest to Pareto's set of solutions. This distance is calculated by $(dAB = sqrt(\,(xB - xA)^2 + (yB - yA)^2\,))$. It is the choice defined as the 'final solution', given in the last row of Tables 7 to 10.

Depending on the manufacturer's factory installation, a core with more than 4 meters in limb height would not be

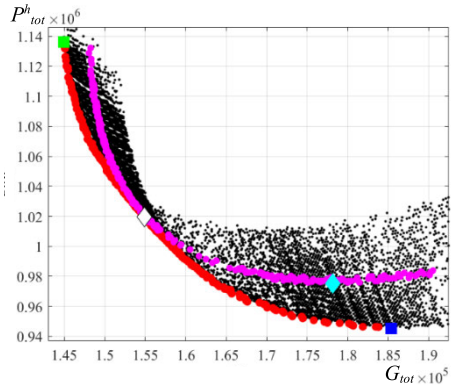

FIGURE 10. The feasible solutions found by the evolutionary constrained multi-objective optimization process for the rectifier delta.

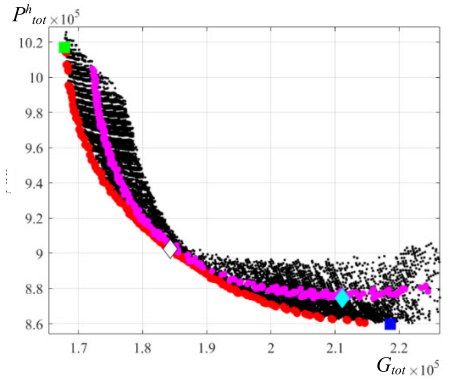

FIGURE 11. The feasible solutions found by the evolutionary constrained multi-objective optimization process for the rectifier star.

feasible, but the exercise is still valid to provide a view of how the different solutions populate the objectives space in two dimensions. The final choice was selected for being the closest to the Pareto's set [31], meaning that it resulted in the best relation between total losses including harmonics and the core and windings weight.

Although, depending on the installation purpose, the objectives and restrictions setup may vary. For instance, if the energy remuneration for a certain system is valued, the operator may prefer a more expensive equipment in terms of material investment, that provides lower losses in operation [9]. On the other hand, if the transformer will be placed on an offshore platform, the total weight and footprint limitations may justify a total loss increase. That choice can result in lighter core and windings, even though may result in other side effects due to the high losses, which can force the designer to select more expensive high-temperature material for windings insulation and oil. Those examples illustrate how the transformer application can affect the objectives selection and the restrictions definition.

V. VALIDATION WITH FINITE ELEMENTS ANALYSIS

The authors considered the winding eddy losses with harmonics a leading parameter to validate the analytic formulation of section III once it depends on the leakage flux and can be a source of deviations in the analysis. Those losses are also frequency dependent and HVDC transformers are subjected to several current harmonic orders. The valve winding is the most stressed one in terms of harmonics, likewise thermally [34]. That reduces the cellulose material life in operation, resulting in possible partial discharges and a future dielectric discharge, or an internal short-circuit failure due to the reduction of the insulation's mechanical strength [35]. That directly impacts the transformer's end of life and its availability in the power system. The validation was done by comparing the valve winding losses calculated by the analytic formulation with a numerical calculation using Finite Elements Method (FEM). Completely distinct methods applied over the same transformer geometry (section II). Since eddy losses depend on the load current frequency, with the harmonics' spectrum (Tables 5 and 6), each ohmic and eddy losses component, can be obtained for the fundamental and all harmonic orders for a specific load profile. The losses with harmonics $\boldsymbol{P_w^{h'}}$, (33), are obtained by adding each loss component, proposed by [36], and [37]:

$$P_w^{h'} = \sum_{h=1}^{49} P_h \tag{33}$$

The currents for each order are injected in the transformer valve winding 2D-FEM model. That calculation methodology differs from a standard design, which would use FEM to define the winding losses and apply F_{WE} on the eddy losses, like in (22).

The core and windings geometry of each type of transformer was generated into a commercial two-dimensional, axisymmetric model FEM software and utilized a time-harmonic solver. The mesh element size was defined based on the penetration depth [38], δ, calculated in (34) and fixed for the 49th harmonic order frequency (2940Hz) [21]. This resulted in an extremely refined mesh, illustrated in Fig. 12, used for all simulations, which would not be needed for lower harmonic frequencies, consuming more computation resources. For the actual study that was not an issue, but that input may be adjusted for other calculations if needed.

The element size is calculated by (35) in [mm] and for 2940Hz it is 0.44986mm, for $\boldsymbol{\sigma_0 = 1 \Big/ 2.11410^{-8}}$ and μ_0 in the SI system. That element size represents less than 1/3 of the winding conductor width, assuring good precision on the results. In the 2D simulation, the control region shall be defined by a maximum element size of two or three layers of the elements, which means, the size should be between 1/2 and 1/3 of the studied dimension [39].

$$\delta = \sqrt{\frac{1}{\pi f \mu_0 \sigma_0}} \tag{34}$$

$$ElemSize = \frac{\delta}{3} 10^3 \tag{35}$$

The valve winding, designed as a helical or a disc winding, had the geometry of each conductor detailed for λ number

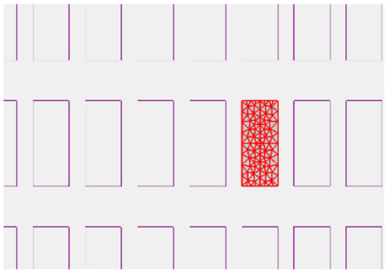

FIGURE 12. Mesh geometry inside a single conductor (cross section view).

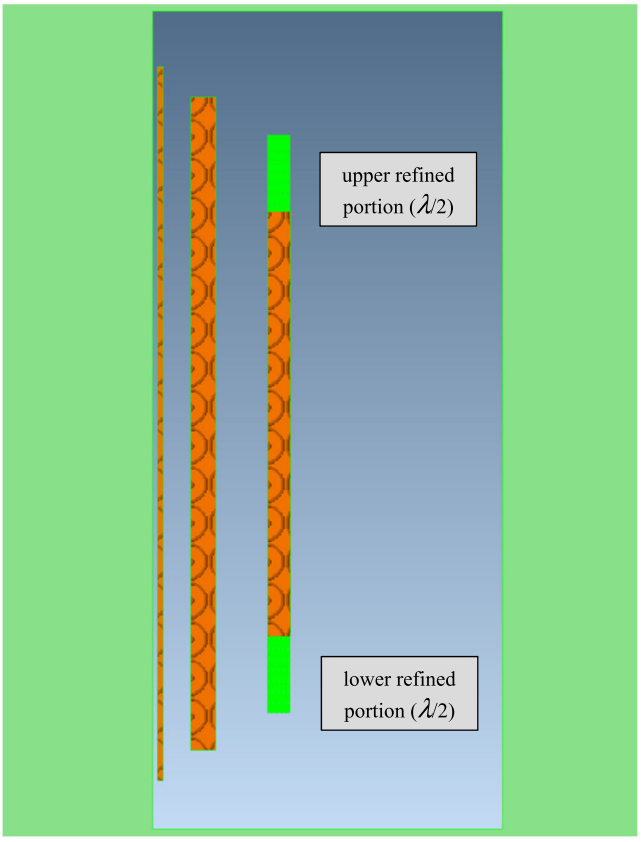

FIGURE 13. Valve winding geometry showing the refined region.

of turns or discs respectively, being λ/2 located on the top and the other half on the winding bottom (Fig. 13). Each conductor of the refined portion was modeled as a solid element and the rest of the winding as a stranded coil, correcting the losses by adding the proportional eddy losses from the analytic calculation.

The first round of simulations was done setting $\lambda = 20$ and then, for one model, a sensibility study, varying λ was performed. The main leakage flux is concentrated between the line (B) and the valve (C) windings and the field line close within the core window, as illustrated in Fig. 14. It is possible to verify that the discs or turns located at the top and bottom winding height suffer a more intensive influence from the magnetic flux. That justifies the need of refining the winding in those regions. The current density and load

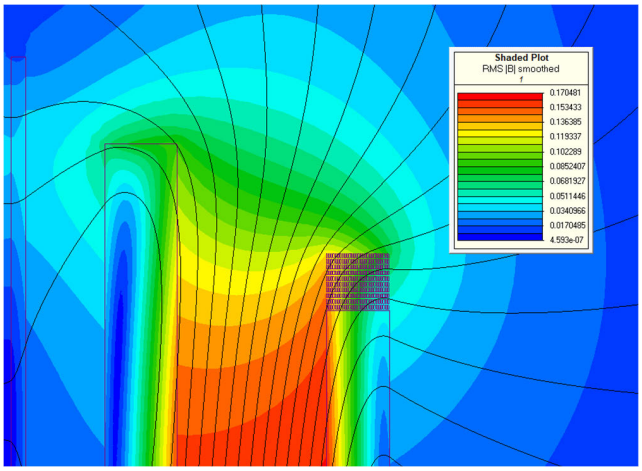

FIGURE 14. Magnetic field lines and magnetic flux B_0 shaded plot.

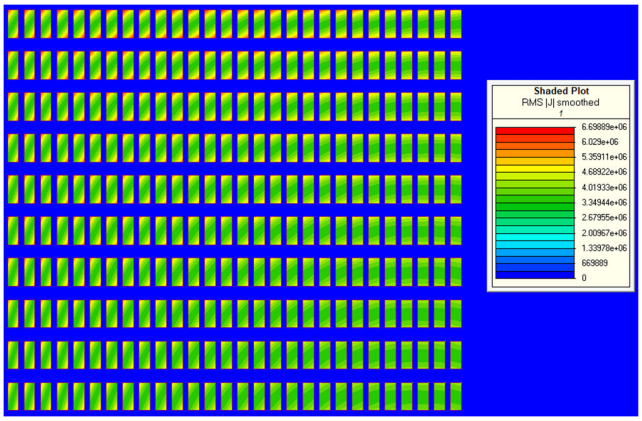

FIGURE 15. Current density distribution in the refined portion shown in Figs. 13 and 14.

losses distribution inside every single conductor of the refined portion show the same behavior in Figs. 15 and 16, stressing more the conductors placed in the inner diameter than the ones in the outermost diameter. That is the expected behavior for that loading analysis [40], illustrating the skin effect inside the material. Before simulating the harmonic losses, the transformer percentage impedance was checked based on the magnetic field energy formulation using (36) [41].

$$U_k\,[\%] = 100\frac{4\pi f\,Energy}{S_{base}} \tag{36}$$

The Energy in [Joules] is taken directly from the FEM simulation and S_{base} is the transformer power base per limb in [VA]. Table 11 presents the calculated percentage impedance for the analytic calculation and the one resulting from the simulation.

That is an important result to assure the simulation is being performed correctly. If the leakage flux energy results in an impedance discrepant from what was expected, it is an indication that the model is not correct.

The four models, rectifier D and Y, and inverter D and Y were simulated setting $\lambda = 20$ and applying each harmonic

TABLE 11. Percentage impedance result.

Station	D/Y	Analytic [%]	FEM [%]
Inverter	D	15.7	15.2
	Y	15.2	14.9
Rectifier	D	15.7	15.1
	Y	15.2	14.9

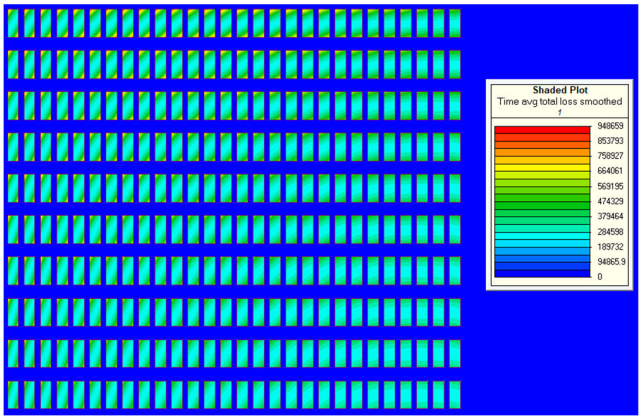

FIGURE 16. Winding losses distribution in the detailed region shown in Figs. 13 and 14.

TABLE 12. Losses results and deviation from the analytic calculation.

Station	D/Y	Analytic losses [kW]	FEM losses [kW]	Deviation [%]
Inverter	D	260.74	249.56	-4.2877
	Y	189.08	182.64	-3.4047
Rectifier	D	271.97	260.36	-4.2685
	Y	198.06	191.45	-3.3366

current into the models and obtaining the losses for the respective frequency, up to the 49th, resulting in the total winding losses $P_w^{h'}$, (33). That result is compared to the analytic calculation P_w^h, obtained from (24). The final losses results are presented below in Fig. 17 and the deviation from both methods, taking the analytic calculation as the reference, is shown in Table 12. The results show a deviation between the two methods of less than 5%. However, the results from Table 9 motivated the authors to investigate if the FEM losses would converge, maintain, or diverge from the analytic calculation when the refined portion increases. That purpose is to verify if the analytic calculation was fair enough when the conductors of the valve winding are represented in more detail.

That investigation took place using the rectifier Y-connected model, varying λ from 6 to 42, in steps of 6 and then two more cases considering $\lambda = 60$ and $\lambda = 78$, with three times the step (Fig. 18).

The more discretized the detailed portion, the lower the deviation between the losses calculated by the two different methodologies, decreasing close to 2%. That result certifies the analytic calculation as a realist method, and that the

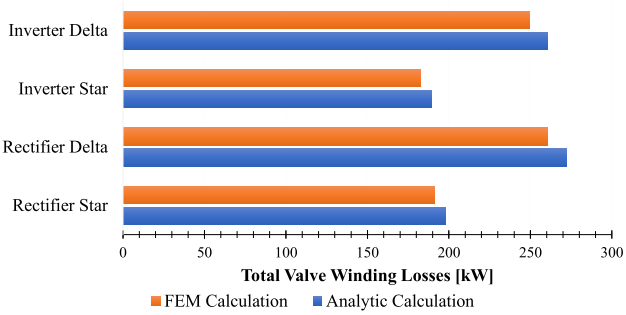

FIGURE 17. Winding losses of the four designs setting $\lambda = 20$.

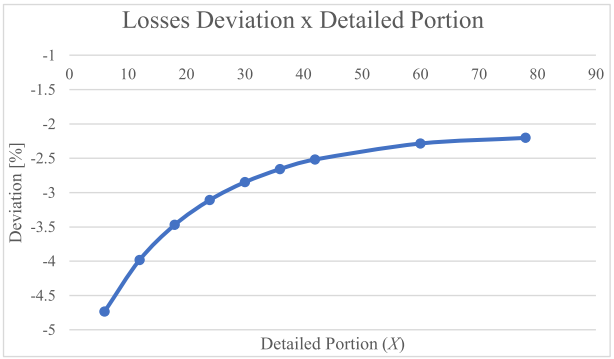

FIGURE 18. Sensibility study for the valve winding losses based on the portion of refined turns shown in Figs. 13 and 14.

formulation presented in section III is reliable for optimizing the converter transformers designs.

VI. CONCLUSION

The formulation proposed in sections II and III was validated in section V by a numerical alternative calculation of the valve winding losses considering harmonics, and by the short-circuit impedance verification, for the four transformers configurations. The results deviation between the two methodologies showed a reduction when the winding conductors' geometry was more detailed, validating the formulation considering the skin effect of the magnetic leakage flux in the extreme winding portions.

In section IV, the formulation is analyzed by a multi-objective optimization, confronting two antagonistic objectives, total losses in operation and active part weight, searching for the optimal solution in a 2-D objective space.

Some secondary tasks obtained by the study shall be highlighted, such as the simulation of the HVDC link in PSCAD, defining the parameters of the transformers, and generating the current harmonics spectrum. Likewise, the creation of an automatic script to draw the core and windings 2-D geometry, input data, and run the FEM program simulation of the harmonic losses.

Future improvements can also be foreseen, once the analytical formulation is simplified and can also be developed considering other parameters such as the core structure, leads connection, solid and liquid insulation, transformer tank, and

other metallic supports. The losses analysis may also include other-eddy losses, which are generated by the magnetic flux impinging all metallic parts, which involves a 3-D analysis, due to the asymmetry of the parts involved in that analysis. The optimization algorithm may also consider other objectives and restrictions, depending on the HVDC converter transformer application.

ACKNOWLEDGMENT

The authors thank Hitachi Energy for the use of the mentioned figures.

REFERENCES

[1] International Energy Agency. (Apr. 2021). *Global Energy Review—2021*. [Online]. Available: https://www.iea.org/reports/global-energy-review-2021
[2] M. V. Czernorucki, M. B. C. Salles, A. S. Melo, E. C. M. da Costa, and L. Piegari, "Effects of the HVDC system on converter transformers," in *Proc. 8th Int. Conf. Renew. Energy Res. Appl. (ICRERA)*, Nov. 2019, pp. 623–630.
[3] M. V. Czernorucki, M. B. C. Salles, E. C. M. Costa, A. S. Melo, and L. Piegari, "Comprehensive overview on HVDC converter transformer design: Additional discussions to the IEC/IEEE 60076-57-129 standard," *IEEE Access*, vol. 10, pp. 40165–40180, 2022.
[4] ANEEL. (2015). *Bipolo HVDC Xingú—Terminal Rio Conversoras, LT-CC ±800 kV Xingú—Terminal Rio, LTs E Equipamentos 500 kV Associados*. [Online]. Available: http://aneel.gov.br/transmissão4
[5] W. Sun, L. Yang, F. Zare, Y. Xia, Li Cheng, and K. Zhou, "3D modeling of an HVDC converter transformer and its application on the electrical field of windings subject to voltage harmonics," *Int. J. Electr. Power Energy Syst.*, vol. 117, pp. 1–10, May 2020.
[6] *PSCAD/EMTDC User's Manual*, Manitoba HVDC Res. Centre, Winnipeg, MB, Canada, 2001.
[7] M. Sanjo, M. Jeffin, J. Sajan, and A. Deepak, "Power electronic on-load tap changer for HVDC converter transformer," *Int. J. Innov. Res. Elect., Electron., Instrum. Control Eng.*, vol. 7, no. 4, pp. 50–58, Apr. 2019.
[8] A. M. Sobrinho, "Uma contribuição aos projetos de transformadores via algoritmos naturais e elementos finitos," Ph.D. dissertation, Departamento de Engenharia Elétrica, Universidade Federal de Uberlândia, Uberlândia, Brazil, Jun. 2019.
[9] W. V. Calil, E. C. M. Costa, and M. B. C. Salles, "Methodology for specification of generator step-up transformers in photovoltaic power plants based on real loading profile," Ph.D. dissertation, Departamento de Engenharia Elétrica, Univ. São Paulo, São Paulo, Brazil, 2020.
[10] Y. Zhao and P. Crossley, "Impact of DC bias on differential protection of converter transformers," *Int. J. Electr. Power Energy Syst.*, vol. 115, Feb. 2020, Art. no. 105426.
[11] Y. Liu, G. Li, L. Guan, and Z. Li, "The single-active-part structure of the UHVDC converter transformer with the UHVAC power grid," *CSEE J. Power Energy Syst.*, vol. 3, no. 3, pp. 243–252, Oct. 2017.
[12] B. A. Thango and P. N. Bokoro, "Stray load loss valuation in electrical transformers: A review," *Energies*, vol. 15, no. 7, p. 2333, Mar. 2022.
[13] Y. Vernay, J. Michel, and J. P. Taisne, "Study and measurement of harmonics emission for the HVDC-LCC French station IFA2000," in *Proc. Int. Conf. Power Syst. Transients*, Perpignan, France, Jun. 2019, pp. 1–6.
[14] G. P. Anuoluwapo, "Power losses in HVDC converter stations," Ph.D. dissertation, Dept. Elect. Eng., Univ. Kwazulu-Natal, Durban, South Africa, Nov. 2018.
[15] Y. Liu, D. Zhang, Z. Li, Q. Huang, M. Li, B. Li, and J. Liu, "Evaluation of the calculation method for stray losses in structural parts of HVDC converter transformers," in *Proc. 5th Int. Conf. Electr. Utility Deregulation Restructuring Power Technol. (DRPT)*, Nov. 2015, pp. 1780–1785.
[16] W. Peng, Q. Liu, Li Liang, W. Jiang, and Z. Zhang, "Design requirement and DC bias analysis on HVDC converter transformer," in *Proc. AESEE E3S Web Conf.*, vol. 257, 2021, p. 01038.
[17] Q. Ni, L. Luo, J. Fan, and Z. Jin, "Harmonic loss analysis of converter transformer in LCL-HVDC system," *Energy Rep.*, vol. 6, pp. 352–357, Dec. 2020.
[18] L. F. Blume, *Transformer Engineering*. Hoboken, NJ, USA: Wiley, 1951.
[19] R. M. D. Vecchio, B. Poulin, P. T. Feghali, D. M. Shah, and R. Ahuj, *Transformer Design Principles: With Applications to Core-Form Power Transformers*. Boca Raton, FL, USA: CRC Press, 2010.
[20] W. Rogowski, "Ueber das streufeld und den streuinduktionskoeffzienten eines transformators mit scheibenwicklung und geteilten endspulen," Ph.D. dissertation, VDI, Mitteilung ueber Forschungsarbeiten auf dem Gebiet des Ingenieurwesens, 1909.
[21] *Power Transformers—Transformers for HVDC Applications*, Standard IEC/IEEE 60076-57-129, Nov. 2017. [Online]. Available: http://webstore.iec.ch/publication/28003
[22] Y. Liu, D. Zhang, Z. Li, Q. Huang, B. Li, M. Li, and J. Liu, "Calculation method of winding eddy-current losses for high-voltage direct current converter transformers," *IET Electr. Power Appl.*, vol. 10, no. 6, pp. 488–497, Jul. 2016.
[23] Y. Wang, W. Zhang, J. Wang, D. Xia, P. Zhang, and J. Li, "Stray loss calculation of HVDC converter transformer," *IEEE Trans. Appl. Supercond.*, vol. 22, no. 3, Jun. 2012, Art. no. 5500604.
[24] *UHV Transmission Technology*, Elsevier Inc., Amsterdam, The Netherlands, 2017, doi: 10.1016/C2013-0-15562-6.
[25] Y. Shuai, X. Han, L. Zhang, C. Yang, X. Hu, and H. Wu, "Major insulation design consideration of converter transformer," in *Proc. Int. Conf. Condition Monitor. Diagnosis (CMD)*, Xi'an, China, Sep. 2016, pp. 1004–1007.
[26] M. Yea, K. J. Han, J. Park, S. Lee, and J. Choi, "Design optimization for the insulation of HVDC converter transformers under composite electric stresses," *IEEE Trans. Dielectr. Electr. Insul.*, vol. 25, no. 1, pp. 253–262, Feb. 2018.
[27] F. Werner and N. Vakhania, *Multicriteria Optimization Pareto: Optimality and Threshold-Optimality*. Rijeka, Croatia: InTech, 2020.
[28] S. L. Avila, "Otimização paramétrica com computação evolutiva," Tech. Rep., 2020.
[29] *Power Transformers—General*, Standard IEC 60076-1, Apr. 2011.
[30] Submódulo 2.6. (Jun. 2021). *Requisitos Mínimos Para Subestações E Seus Equipamentos*. ONS. [Online]. Available: http://ons.org.br
[31] J. Liang, X. Ban, K. Yu, B. Qu, K. Qiao, C. Yue, K. Chen, and K. C. Tan, "A survey on evolutionary constrained multi-objective optimization," *IEEE Trans. Evol. Comput.*, early access, Mar. 1, 2022, doi: 10.1109/TEVC.2022.3155533.
[32] L.-X. Zhang, X.-Y. Kong, S.-S. Zhang, Z. Zhang, W. Lu, and X.-M. Zhang, "Optimization arrangement of angle rings in converter transformer valve winding end insulation structure," in *Proc. IEEE Int. Conf. High Voltage Eng. Appl. (ICHVE)*, Sep. 2020, pp. 1–4, doi: 10.1109/ICHVE49031.2020.9279713.
[33] S. Yadav and R. K. Mehta, "Modelling of magnetostrictive vibration and acoustics in converter transformer," *IET Electr. Power Appl.*, vol. 15, no. 3, pp. 332–347, Mar. 2021.
[34] *HVDC Converter Transformer Failure Survey Results From 2013 to 2020*, CIGRE, Paris, France, Dec. 2021.
[35] P. Jiang, Z. Zhang, Z. Dong, Y. Wu, R. Xiao, J. Deng, and Z. Pan, "Research on distribution characteristics of vibration signals of ±500 kV HVDC converter transformer winding based on load test," *Int. J. Electr. Power Energy Syst.*, vol. 132, Nov. 2021, Art. no. 107200.
[36] B. S. Ram, J. A. C. Forrest, and G. W. Swift, "Effects of harmonics on converter transformer load losses," *IEEE Trans. Power Del.*, vol. PD-3, no. 3, pp. 1059–1066, Jul. 1988.
[37] Q. Ni, L. Luo, J. Fan, and Z. Jin, "Harmonic loss analysis of converter transformer in LCL-HVDC system," in *Proc. 7th Int. Conf. Power Energy Syst. Eng.*, vol. 6. Fukuoka, Japan, Sep. 2020, pp. 352–357.
[38] D. K. Cheng, *Field and Wave Electromagnetics*, 2nd ed. Reading, MA, USA: Addison-Wesley, 1989.
[39] D. A. Lowther and P. P. Silvester, *Computer—Aided Design in Magnetics*. Berlin, Germany: Springer, 1986.
[40] M. C. Mgunda, "Optimization of power transformer design: Losses, voltage regulation and tests," *J. Power Energy Eng.*, vol. 5, no. 2, pp. 45–74, 2017.
[41] M. L. Magid, *Electromagnetic Fields, Energy and Waves*. Hoboken, NJ, USA: Wiley, 1972.

MARCOS V. CZERNORUCKI was born in São Paulo, Brazil, in 1975. He is currently pursuing the Ph.D. degree in electrical engineering with the Polytechnic School of the University of São Paulo. His research interests include different types of transformers, such as industrial, phase-shifters, and converter transformers, and their interaction with the power system under prospective designs. He is a member of Cigré Brazil, actively participating on the working group A2.09 and on the standards revision of the Brazilian Technical Standard Association.

MAURICIO BARBOSA DE CAMARGO SALLES (Member, IEEE) received the Ph.D. degree from the University of São Paulo (USP), Brazil, in 2009. From 2006 to 2008, he was with the Research Team of the Institute of Electrical Machines, RWTH Aachen University. He has been an Assistant Professor with the Laboratory of Advanced Electric Grids, Polytechnic School of the University of São Paulo, São Paulo, Brazil, since 2010. From 2014 to 2015, he was a Visiting Scholar with the Harvard John A. Paulson School of Engineering and Applied Sciences. His research interests include distributed generation, power system dynamics, control and stability, renewable energy, energy storage, and electricity markets.

SÉRGIO LUCIANO AVILA received the dual Ph.D. degrees from the Ecole Centrale de Lyon (ECL), Lyon, France, and UFSC, in 2009. From 2006 to 2007, he was with the Research Team of the Grenoble Institute of Technology (Grenoble INP). He has been an Associate Professor with the Laboratory of Applied Scientific Computing (PECCE), Federal Institute of Santa Catarina (IFSC), Florianópolis, Brazil, since 2010. From 2017 to 2018, he was a Visiting Scholar with the Polytechnic School of the University of São Paulo, São Paulo, Brazil. Currently, he works on solutions for monitoring and predicting behavior in machines and electrical systems, which involves instrumentation, numerical modeling, optimization, and computational intelligence algorithms.

FELIPE ALVES SOBRINHO received the degree in electrical engineering from Brasilia University, in 2004. In 2002, he started working with power systems analysis and studies as a Trainee with Eletronorte, where he worked as a Planning Engineer for the following 12 years. In 2014, he joined ABB to work with HVDC first in Guarulhos, Brazil, and then in Ludvika, Sweden. Since 2022, he has been working as a Principal Consultant with the Power Consulting Team, Hitachi Energy Ltda., Raleigh, NC, USA, focusing mainly on new HVDC projects.

WILERSON W. CALIL received the B.Sc. degree in electrotechnical engineering from the Mauá School of Engineering, São Paulo, Brazil, in 2005, and the M.Sc. and Ph.D. degrees in electrical engineering from the University of São Paulo, São Paulo, in 2009 and 2020, respectively. He is currently pursuing the Ph.D. degree in electrical engineering with the Polytechnic School of the University of São Paulo. Since 2004, he has been working with Hitachi Energy Ltda., where he also holds the position of a Principal Project Engineer. His research interests include applied electromagnetism, magnetic and thermal simulations, power systems modeling, power transformer design, transformers applied with renewable sources, and high-voltage techniques for experimental analysis. In addition, he is an active member of the International Council on Large Electric Systems (Cigre) and has several internationally renowned publications.

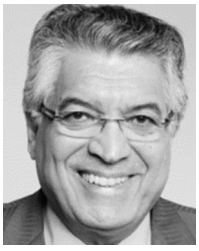

JOSÉ ROBERTO CARDOSO (Life Member, IEEE) was born in Marilia, São Paulo, Brazil, in 1949. He received the B.S., M.S., and Ph.D. degrees in electrical engineering from the Polytechnic School, University of São Paulo, São Paulo, in 1974, 1979, and 1986, respectively. Since 1999, he has been a Professor with the Electrical Energy and Automation Engineering Department, Polytechnic School, University of São Paulo. He is currently the President of the SBMAG—Brazilian Electromagnetics Society and the former Dean of the Polytechnic School of the University of São Paulo. He is the Founder of the LMAG—the Electromagnetic Applied Laboratory. He is the author of four books and more than 70 articles and has guided more than 40 theses/dissertations. His research interests include numerical methods for electromagnetics, theoretical electromagnetics, electrical machines, electromechanical biomedical application, and electrical railway research and engineering education. He was a recipient of the 2013 Emeritus Engineer of the Year in São Paulo. He was awarded Doctor Honoris Causa by the Grenoble-INP Institute of Engineering, France, in 2019.